Impact Damage Detection Limits of Microwave NDE Technique for Polymer Composites

KATHERINE BERKOWITZ, RISHABH D. GUHA,
OGHENEOVO IDOLOR, MARK PANKOW
and LANDON GRACE

ABSTRACT

Despite recent advances, the need for improved non-destructive evaluation (NDE) techniques to detect and quantify early-stage damage in polymer matrix composites remains critical. A recently developed microwave based NDE technique which capitalizes on the ubiquitous presence of moisture within a polymer matrix has yielded positive results. The chemical state of moisture directly affects dielectric properties of a polymer matrix composite. Thus, the preferential diffusion of 'free' water into microcracks and voids associated with physical damage allows for damage detection through spatial permittivity mapping using techniques that are sensitive to moisture content and molecular water state. While it has been demonstrated that the method can detect damage at low levels of moisture and impact damage, the specific parameters under which the technique will accurately and reliably capture damage within a composite are unknown. The three variables affecting the performance of the method to detect impact damage are moisture content, extent of damage, and resolution of the dielectric scanning technique. Here, we report on the impact of the latter as a function of the two environmental variables (moisture and damage extent). To understand limits and optimize execution of the technique, the interrelationships between each of the variables must be explored. This study investigates the relationship between moisture content and scan resolution. Two BMI/quartz laminates were impacted at 9 Joules to induce barely visible impact damage. The specimens were inspected at a variety of gravimetric moisture levels, and several variations of the spatial permittivity map were created for each moisture level. Detection standards for the technique were investigated based on moisture content and desired scan accuracy; findings showed at 0.05-0.4% moisture content (by wt.) the technique can detect damage location and size with a minimum of 88% accuracy. Pareto frontiers were generated at each moisture level to optimize scan speed and accuracy.

Katherine Berkowitz, Rishabh D Guha, Ogheneovo Idolor, Mark Pankow, Landon Grace, North Carolina State University, 1840 Entrepreneur Dr, Raleigh, NC 27695

INTRODUCTION

The use of polymer matrix composites (PMCs) has expanded rapidly in several relevant industries such as aerospace, renewable energy, transportation, oil and gas, civil structures, and defense [1]–[3]. These materials are replacing traditional materials such as metals due to their superior mechanical properties and other benefits, such as improved corrosion resistance, part count reduction, and desirable dielectric properties [4]–[6]. Perhaps most importantly, composites materials can be tailored with varying degrees of anisotropy to meet required part strength and stiffness in multiple directions. This attribute can contribute to improved weight and optimal structural aerodynamics [7]. However, anisotropy of PMCs increases the complexity of damage mechanisms when compared to homogenous, traditional materials like metals [1]. Internal defects and damage can be generated in a composite either during manufacturing or in-service; both of which pose threats to the structural integrity of a laminate. Flaws induced during manufacturing can create voids or resin-rich regions, inclusions, laminate warping and more resulting in a reduction of effective strength and thickness. While in service, composites can be subjected to static and cyclic loading, as well as impact forces. On top of mechanical loading, in-service composites may experience environmental damage due to high temperatures, humidity, and chemicals [8]. The four major types of damage resulting from these forces are matrix cracking, interfacial debonding, delaminations and fiber breakage [8], [9]. A composite part will fail due to the accumulation of basic rupture mechanisms like these. Typically, the damage initiates at the nano- or micro-scale as the cross-linked networks of the polymer matrix begin to yield. It then propagates through the micro- and meso-scale with matrix cracking and interfacial debonding, eventually leading to delaminations, fiber breakage, and ultimately part failure on the macro-scale [1]. Due to non-homogeneity of PMCs, damage can accumulate at multiple sites occurring at different scales, which makes it difficult but crucial to identify and track each site as early as possible.

Much of the damage sustained due to mechanical or environmental loads is non-visible or barely visible due to its small length scale or location within the structure. Low-velocity impacts, for example, can cause a network of matrix cracking and delaminations within a laminate without any indication on the top surface [7], [10]. Since microcracks and other damage can cause catastrophic and expensive structural failure, robust and reliable non-destructive evaluation (NDE) techniques to detect early-stage damage sites are critical. There are several techniques that have been well-evaluated for use on PMCs, such as visual inspection, ultrasonic testing, thermography, and others [11]–[15]. While these methods have been reasonably effective, it is found they have difficulty characterizing combined environmental-mechanical effects and damage below the micron-scale. These are severely limiting factors in detection of early-stage damage and tracking damage progression, both of which are fundamental in preventing catastrophic failure [15].

The use of microwaves, through resonant cavity, free space, or transmission line methods as an NDE technique has proven moderately effective, efficiently inspecting lossless and low loss dielectric materials due to their low attenuation [16]. To potentially address shortcomings of other common NDE methods, our lab has recently proposed a modified microwave NDE technique that capitalizes on the ubiquitous presence of moisture within a non-conductive PMC [17] and uses said moisture as a damage "imaging agent" [6], [18]–[22]. Moisture exists in different chemical states in a

composite; if the molecules are connected to the network via secondary bonding interactions it is considered 'bound' water and is severely restricted from aligning to an applied electromagnetic field. Without the chemical constraints, water near damage sites can be considered 'free' as they quickly align to applied electromagnetic fields [23], [24]. The dielectric properties of bound versus free water differ significantly, restriction in rotation leads to a relative permittivity of about 3 in bound water while free water has a relative permittivity of about 80 [25]. The accumulation of damage in a structure creates pathways of microcracks and voids for free water to occupy, allowing for detection of damage through spatial relative permittivity maps. Our previous work has demonstrated the capability of impact damage detection across several impact energies and gravimetric moisture contents [6], [19], but specific parameters under which the technique can accurately detect and locate damage are unknown.

There are three key variables which affect the accuracy and detectability of the developed dielectric method: gravimetric moisture content, extent of damage (or damage length scale), and grid spacing of the spatial permittivity map. Identification of parameters that the technique can be used under is essential for transition to commercial and industrial use, where moisture content and damage extent may be unknown. For example, nano- or micro-scale damage might require a higher moisture content or higher scan resolution for detection, as opposed to meso-scale damage which might only require very low levels of moisture. As the technique starts competing with existing methods, it also needs to be optimized with respect to scan time, which is inversely proportional to scan resolution. Ultrasonic scans, for example, are commonly used in industry and are currently much faster than the dielectric technique to scan identical areas [14]. The purpose of this experiment is to study the effects of moisture content and grid spacing on scan accuracy. Impact energy will be held constant and its interrelationships with moisture content and scan resolution will be explored in further experiments. In addition to quantification of scan accuracy, multi-objective optimization of the technique is explored to minimize scan time while maximizing scan accuracy.

METHOD

Specimen Preparation

Two test specimens were cut from a twelve-ply quartz-fiber reinforced bismaleimide (BMI) laminate using a wet diamond saw. Specimen dimensions were approximately 132mm x 75mm, varying by ± 5%. Average sample thickness was 2.61mm. Laminate properties were obtained via resin burn-off in accordance with ASTM D3171 [26]; 15 specimens were maintained at 800°C until all BMI was removed. Estimated fiber, matrix, and void contents are given in Table I.

TABLE I: BMI/QUARTZ LAMINATE PROPERTIES

Property	Mean (%)	Standard Deviation (%)
Fiber Volume Fraction	59.41	0.149
Matrix Volume Fraction	40.27	0.144
Void Volume Fraction	0.32	0.045

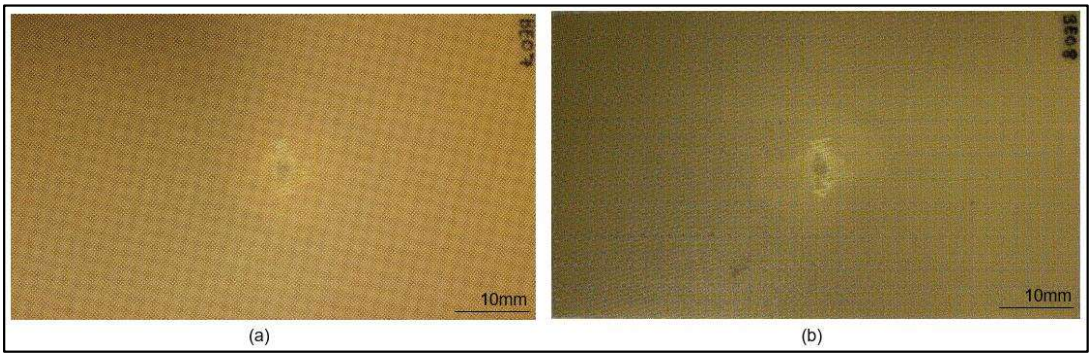

Figure 1: Image of 9J central impact damage in (a) sample 1 and (b) sample 2

The test specimens were dried in a vacuum oven at 65°C until dry, in accordance with ASTM D5229 [27]. Once dry, each specimen was subjected to impact damage via drop tower. A hemispherical striker tip of 9mm diameter was attached to a crosshead and dropped at the appropriate height to induce 9 Joules of impact damage at the center of each specimen. Low-velocity impact damage was chosen to replicate the effect of damage from the likes of hail or a dropped tool. This energy level is one that would induce barely visible damage when the laminate is coated, requiring the use of an NDE technique for damage detection. Images of the damaged samples are shown in Figure 1.

Moisture Contamination

Specimen weight data was recorded prior to beginning moisture uptake. The samples were then exposed to ambient laboratory air and gravimetric moisture uptake was monitored periodically using a high precision analytical balance. Humidity was monitored using an Elitech GSP-6G digital temperature and humidity sensor, and relative humidity generally fluctuated between 55-60%.

Dielectric Mapping Technique

To obtain dielectric measurements of each specimen at microwave frequencies, a split-post dielectric resonator (SPDR) manufactured by QWED© of Warsaw, Poland was linked to an Agilent programmable vector network analyzer (VNA) via high precision coaxial cables. This setup permits the measurement of bulk relative permittivity with uncertainty of about 0.3% [28]. It also enables the ability to detect small changes on the order of 10^{-3}. Before measurements were taken, the system was calibrated via adjustment of scattering parameters S11, S22, and S21, each respectively representing the magnitude of the reflected signal at port 1, port 2, and the transmitted signal from port 1 to port 2. The position of the coupling loops within the resonant cavity were modified such that the minimum gain of S11 and S22 were equal, and subsequently the gain of S21 was adjusted to equal -40 dB. Once calibrated, the resonant frequency and the quality factor of the empty resonator were recorded at 2.48 GHz for use in the calculation of the relative permittivity. As the specimen is inserted, the shift in resonant frequency is measured by the VNA. These values, along with specimen thickness, are used to determine the real part of relative permittivity (ε'_r) of the specimen according to Equation 1 [28].

$$\varepsilon'_r = 1 + \frac{f_0 - f_s}{h\, f_0\, K_\varepsilon(\varepsilon'_r, h)} \quad (1)$$

where

f_0 is resonant frequency of empty SPDR

f_s is resonant frequency with the dielectric specimen inserted

h is sample thickness

K_ε is a function of ε'_r and h, documented in a table unique to each SPDR and provided by the manufacturer

To create the spatial permittivity maps, a setup of NEMA-17 stepper motors, linear screw actuators, and A4988 motor drivers is used (Fig. 2). The setup is controlled by an Arduino MEGA 2560 board coupled with a MATLAB script to concurrently move the specimen within the resonant cavity and use the VNA to take dielectric measurements at each point. The script intakes the length and width of the specimen, along with the desired step sizes in the x and y directions. The specimen is then scanned while ensuring the entirety of the resonant cavity is filled, resulting in scan sizes smaller than the actual specimen. Equivalent scan size is shown in Figure 3. A variety of maps with differing resolutions can be created by choosing different step sizes in the x and y directions. For this experiment, we chose to explore the accuracy of five different step sizes across a variety of moisture contents. Table II provides a description of each of scan used from highest to lowest resolution, with resolution quantified by the average distance from one measurement to its surrounding measurements. Illustrations of each of the step sizes used are shown in Figure 4.

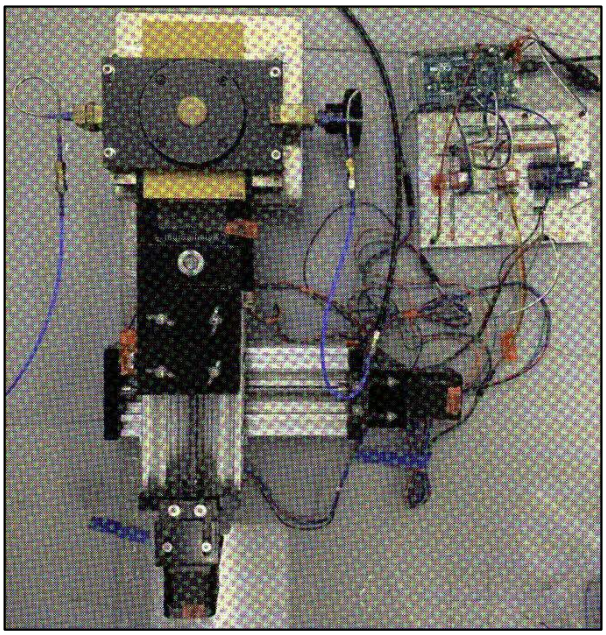

Figure 2: Actuator and stepper motor device to move specimens within the resonant cavity

TABLE II: DESCRIPTION OF SCAN RESOLUTIONS USED

Scan Label	X step size (mm)	Y step size (mm)	Total Number of Points	Average Distance to Surrounding Points (mm)
A	1	1	1638	1.21
B	2	1	858	1.62
C	5	2	195	4.44
D	5	5	80	6.04
E	10	5	48	9.03

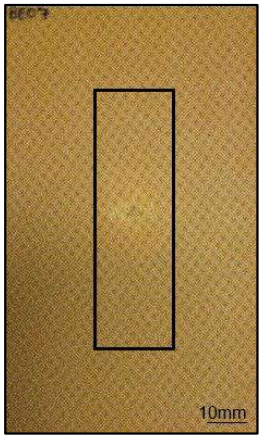

Figure 3: Sample 1 with black box indicating scan area

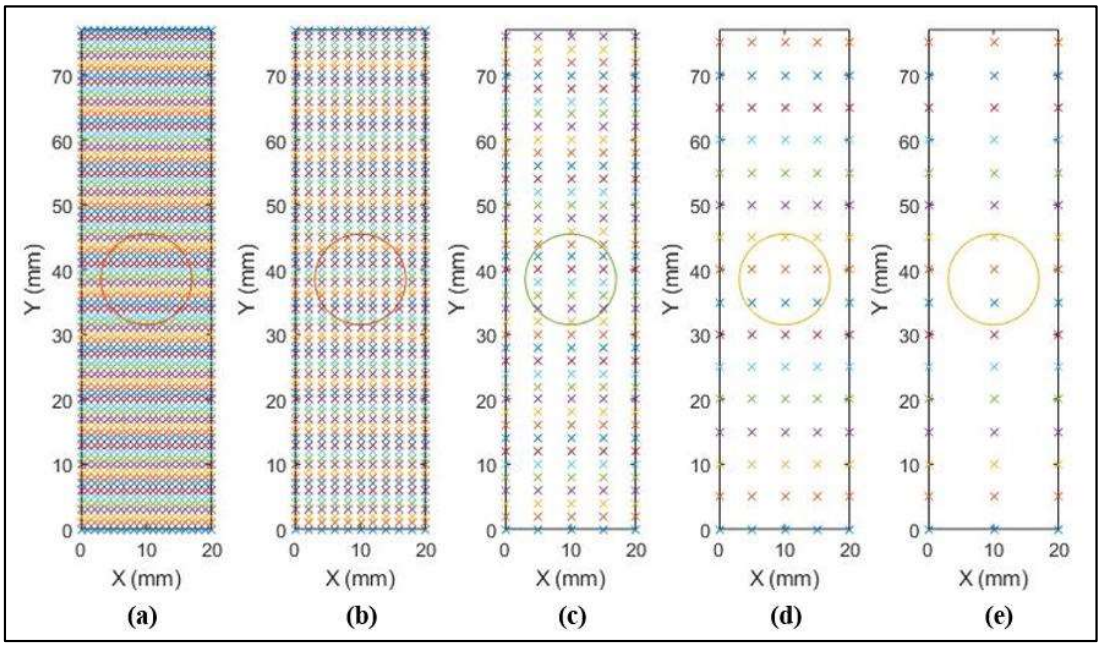

Figure 4: Each of the five separate scan resolutions explored, where each "x" marks a dielectric measurement, and the circle is indicative of approximate damage boundary. Scan labels in the figure represent those described in Table II, i.e., Figure 4(a) shows scan label A

RESULTS AND DISCUSSION

Dielectric measurement scans of each of the five scan resolutions were taken at a variety of gravimetric moisture contents for both specimens. For each sample, post-impact baseline scans were taken at 0% moisture. This dry baseline was subsequently subtracted from each wet scan to account for permittivity variation due to thickness. Gravimetric moisture contents at which scans were taken for each sample are shown in Table III.

TABLE III: MOISTURE CONTENTS AT EACH SCAN INTERVAL

Specimen	M1	M2	M3	M4	M5	M6
1	0.1%	0.18%	0.21%	0.28%	0.32%	0.37%
2	0.04%	0.14%	0.225%	0.32%	0.35%	0.4%

The data was then analyzed using a MATLAB script. Scans of resolutions B, C, D, and E were first interpolated to the same number of measurements as scan resolution A. Maximum permittivity was identified and a threshold "damaged" permittivity value was determined as 95% of the maximum. Every point in each scan was then labeled as damaged if above the threshold, or undamaged if below. Example scans of different resolutions at the same moisture content are shown in Figure 5, and scans of different moisture contents at the same resolution are shown in Figure 6. Red is representative of undamaged points, while blue represents damaged points.

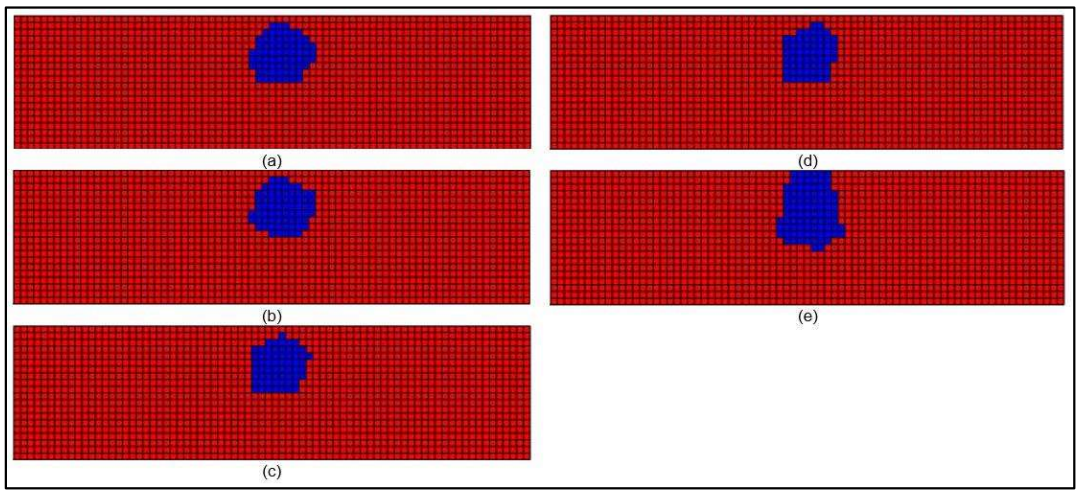

Figure 5: Scans of specimen 1 at each of the five scan resolutions (a) A, (b) B, (c) C, (d) D, and (e) E, at moisture measurement M5, or 0.32%.

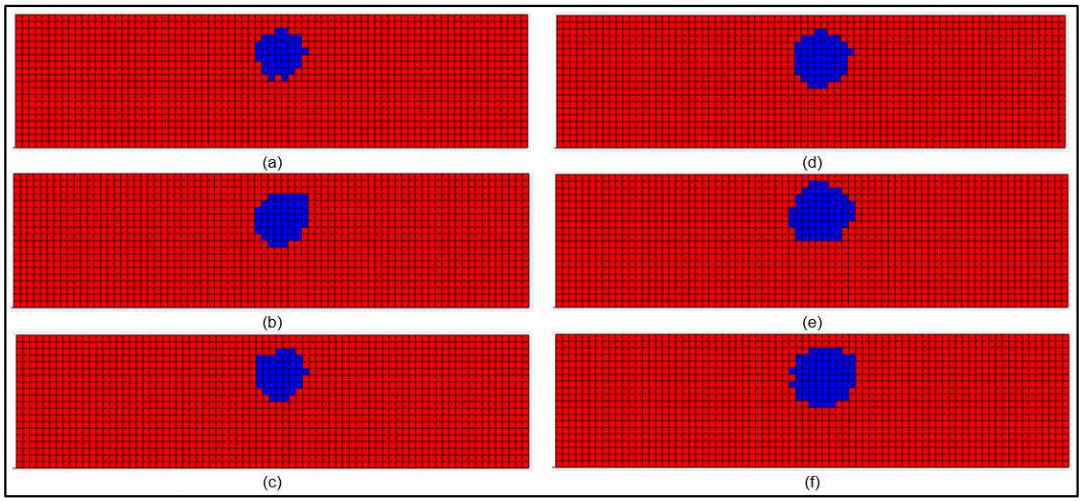

Figure 6: Scans of specimen 1 at (a) M1, (b) M2, (c) M3, (d) M4, (e) M5, and (f) M6 at the highest scan resolution (scan label A).

Qualitatively, the accuracy of the technique appears to improve with a heightened scan resolution or with increased moisture content. The technique is capable of detecting the presence of a circular-shaped impact damage at all moisture contents and resolutions tested. To quantitatively evaluate these observations, every point in a scan was compared to each pixel in the image of actual damage. To create an equivalent scan for the "actual damage", the back of each specimen was photographed and cropped to represent the scan area. Visible damage on the back of the sample was chosen due to the pine tree nature of damage distribution of impact damage to a PMC, with the damage boundary widening through the thickness of the laminate. These images were processed using the MATLAB imaging toolbox; contour maps were created to outline the actual damage in the specimen. The map was then manually overlayed with two colors to indicate damaged and undamaged areas, and the number of pixels were changed to equal the number of dielectric measurements in scan resolution A (Fig. 7). If the scan prediction matched the actual image, it was counted as a correct measurement. Through this process, the scan accuracy was quantified by percentage of correct measurements.

Figures 8 and 9 display plots of scan accuracy as a function of moisture content for each scan resolution and specimen. Trends in Figure 8, showing data for sample 1, support the previously stated qualitative analysis. For each scan resolution, there is a slight increase in scan accuracy as moisture increases with some slight deviations from linearity, especially within the lower scan resolutions. Because grid spacing and total number of measurements of D (5x5mm) and E (10x5mm) is much lower than other resolutions, these low-resolution scans tend to over or underestimate data more frequently, leading to a more variable scan accuracy regardless of moisture content. Figure 9 depicts that sample 2 data has the same general trend of an increase in accuracy with increasing moisture content, except a slight dip which is observed at M5 (0.35% by wt.) and a small bounce back at M6 (0.4% by wt.). It is possible that at higher moisture contents accuracy may begin to drop off as ingress of water continues and damage sites become saturated; continued experiments with readings of moisture contents up to 1-2% by weight will provide insight into whether this trendline may be more parabolic than indicated here. It is also worth noting that there is little difference

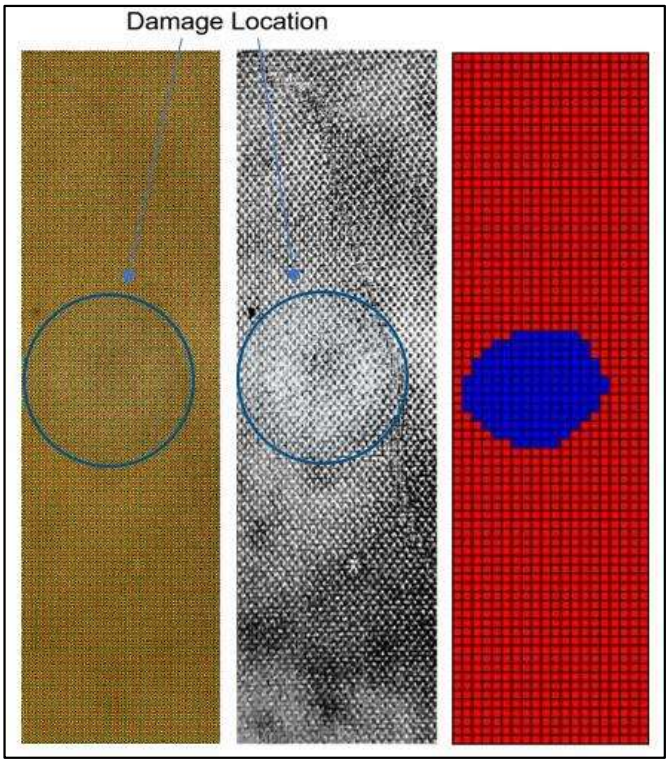

Figure 7: Photograph (left), contour plot (middle) and representative scan (right) of actual damage

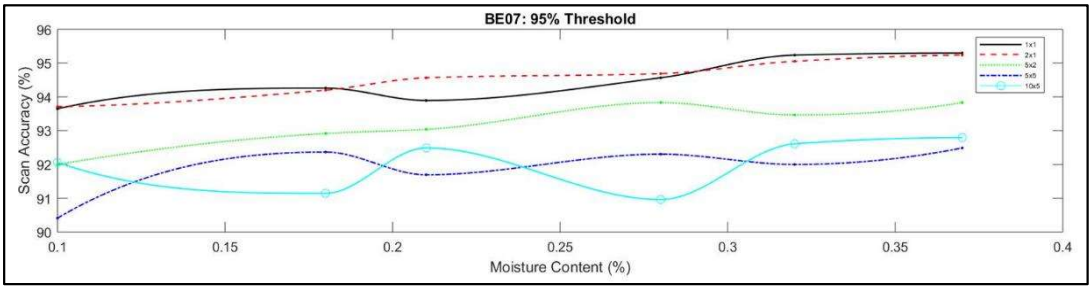

Figure 8: Scan accuracy as a function of moisture content for sample 1

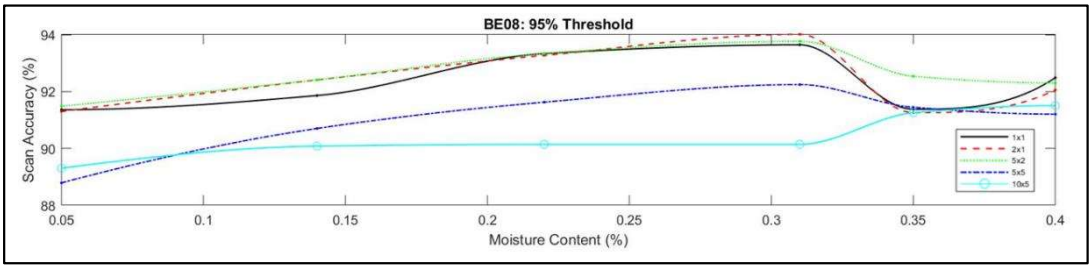

Figure 9: Scan accuracy as a function of moisture content for sample 2

in accuracy between the highest two scan resolutions, suggesting that a resolution higher than B will result in negligible scan accuracy improvement.

Figures 10 and 11 provide another perspective to analyze the data; scan accuracy was also analyzed as a function of scan resolution. Resolution was quantified by a measurement's average distance to its surrounding measurements. Distance increases as scan resolution decreases; Table II provides exact data points for each scan resolution.

Plots for both specimens generally show a decrease in accuracy with a decrease in scan resolution. In both graphs, the M1 data does not have as clear of a trend. This is likely due to the very low level of moisture in the laminate; fewer molecules of free water within the damaged sites will likely lead to low accuracy. Another point to take into consideration when observing these trends are the low number of data points collected. While trends match expectations (accuracy decreases with scan resolution), these trendlines were created using only five data points. Number of scans of different resolutions at each moisture content had to be limited due to time constraints. Completing all five scans took approximately six hours; adding other scan sizes would have been difficult to ensure that each scan was still at the original moisture content.

Because time is a substantial limiting factor in the use of this technique when compared to ultrasound and other commonly used methods, it is important to optimize the procedure by minimizing scan time—which is directly proportional to number of total dielectric measurements. However, minimizing number of measurements means minimizing scan resolution, which will negatively affect scan accuracy as shown in Figures 8 and 9. With two conflicting objectives, we can formulate a multi-objective design optimization problem and probe into the possibility of detection parameters and optimization based on evaluation requirements.

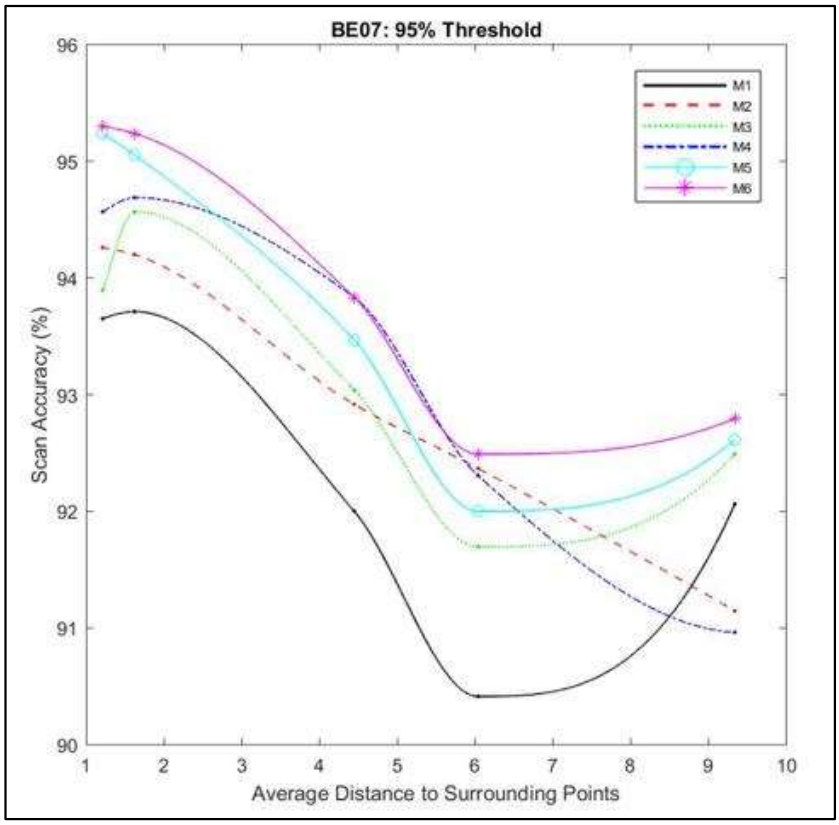

Figure 10: Scan accuracy as a function of scan resolution for sample 1

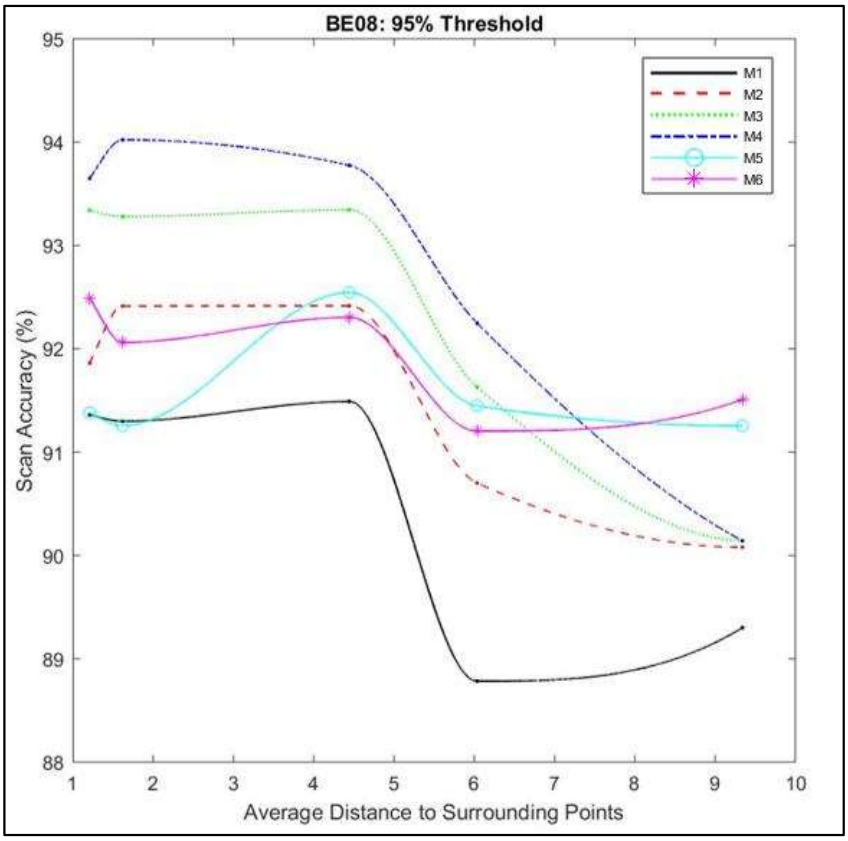

Figure 11: Scan accuracy as a function of scan resolution for sample 2

Multi-Objective Design Optimization

The need to utilize multi-objective optimization arises from conflicting objective functions in minimizing scan time and maximizing scan accuracy with variables of step size in the x and y directions. Because of this, a single unique solution does not exist with respect to both objectives [29]. Instead, a Pareto frontier can be generated with many efficient solutions. These solutions are ones in which there cannot be an increase obtained in one objective function without a subsequent decrease in another objective function. Objective 1 (F_1) is to minimize scan time, shown as Equation 2. Objective 2 (F_2) is to minimize scan error, defined as 1 – scan accuracy. The relationship between scan accuracy and step sizes was characterized using power trendlines for each of the moisture measurements in Figure 8, shown as Equations 3-8. A Pareto frontier was generated for each of the six moisture contents by using the function 'gamultiobj' as part of the MATLAB Global Optimization Toolbox. This function utilizes a genetic algorithm to find the Pareto set given population size, pareto fraction, and constraints. Step sizes in the x and y direction were both subject to the constraints 0.5 mm $\leq x_i \leq$ 10 mm; anything outside of these bounds would be either too long regarding scan time or below a reasonable scan accuracy. Figure 12 displays Pareto sets for each moisture content.

Objective 1:

$$F_1 = 0.084 * \left[\left[\frac{77}{x_1} + 1\right] * \left[\frac{20}{x_2} + 1\right]\right] + 12.666 \quad (2)$$

Objective 2:

Moisture Reading		
M1	$F_2 = 1 - 0.93940(D)^{-0.014}$	(3)
M2	$F_2 = 1 - 0.9480(D)^{-0.012}$	(4)
M3	$F_2 = 1 - 0.9450(D)^{-0.018}$	(5)
M4	$F_2 = 1 - 0.9538(D)^{-0.017}$	(6)
M5	$F_2 = 1 - 0.9561(D)^{-0.015}$	(7)
M6	$F_2 = 1 - 0.9572(D)^{-0.015}$	(8)

where D represents average distance to surrounding points:

$$D = 0.25[x_1 + x_2 + 2\sqrt{x_1^2 + x_2^2}\,] \quad (9)$$

and

x_1 is step size in the x-direction
x_2 is step size in the y-direction

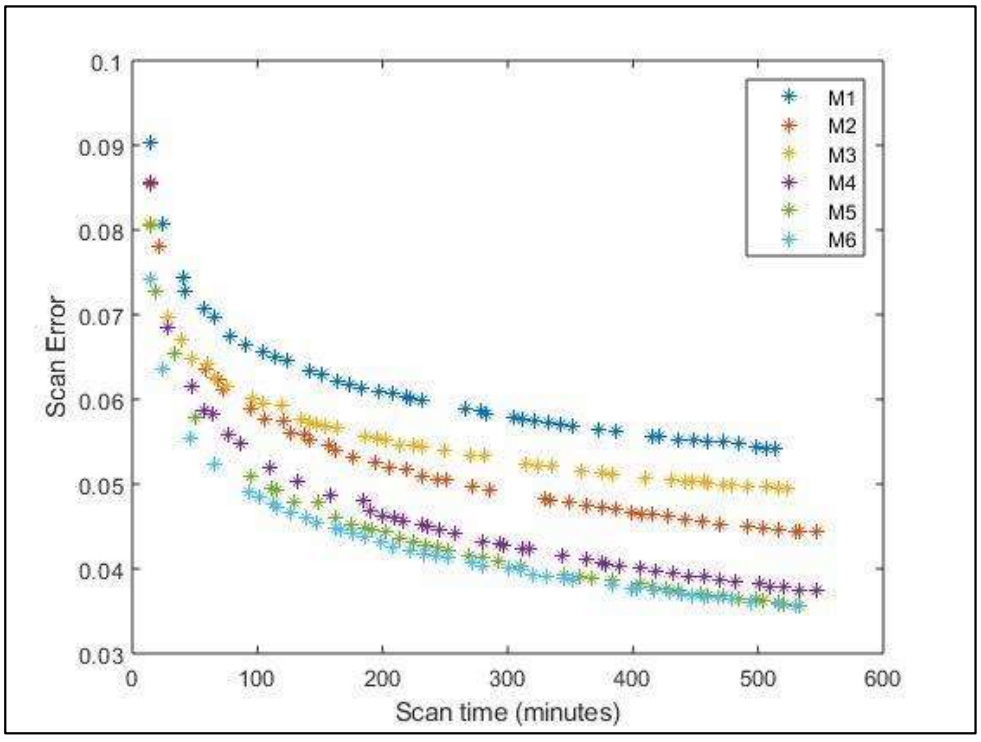

Figure 12: Compiled Pareto frontiers for each moisture content

While still in the early stages, generating Pareto sets across a variety of moisture contents offers exceptionally useful information for a potential transition to industry use. Figure 12 clearly shows that with an increase in moisture, scan time (or resolution) can be sacrificed without sacrificing integrity of scan accuracy. Once the effect of damage extent is incorporated in further experiments, Pareto sets across large sets of data for different materials have the potential to act as reference charts for an operator analyzing an in-service structure. Utilizing knowledge of what scale of damage to detect is desirable, along with desired scan accuracy, an optimal solution of x and y step sizes can be used to minimize scan time. Additionally, if little to no knowledge of moisture content is available, these plots can be used to estimate the required scan resolution for an average moisture content. It is necessary to continue to add higher moisture contents to this plot, however, and those results will be reported in future studies.

CONCLUSION

The detection limits of a novel microwave NDE technique utilizing moisture as an imaging agent were explored in relation to two of three influential variables, moisture content and scan resolution. Polymer composites were impacted and subjected to moisture contamination by humid air. As gravimetric moisture content increased, spatial permittivity maps of varying resolutions were created periodically by using a stepper motor device to move the sample within a split post dielectric resonator. Scans were compared to images of the actual damage, and accuracy of the scan was quantified by comparing individual measurements to pixels. It was shown that the method detected a circular-shaped central damage site regardless of moisture content and scan resolution. The least accurate scan was 88.8% accurate at 0.05% moisture by wt. using a 5x5mm resolution, and the most accurate scan was 95.3% accurate at 0.37% moisture by wt. using a 1x1mm resolution. Accuracy was then plotted with respect to moisture content as well as scan resolution. It was observed that accuracy generally improved with higher moisture content and scan resolution, although it was noted that scans at higher moisture contents are required before making a definitive conclusion. There was also a negligible difference in scan accuracy between the highest two scan resolutions, suggesting it may not be necessary to use a 1mm step size with damage of this extent. However, the relationship between scan resolution and damage extent will be explored in a future study and smaller damage, such as 1 Joule, will likely require higher resolution.

Pareto frontiers were developed for a multi-objective optimization problem with objectives to minimize scan error while minimizing scan time. 42 efficient solutions were found for each moisture content, and the curve will prove useful in determining the fastest step size to use while maintaining the desired scan accuracy. Future experiments will incorporate information gained from the relationship between scale of damage and scan resolution, and ideally create a parameter chart that can be used for operator assistance in choosing the scan resolution based on known and unknown factors.

ACKNOWLEDGEMENTS

This material is based upon work partially supported by the National Science Foundation under Grant No. CMMI-175482.

REFERENCES

[1] B. Wang, S. Zhong, T. L. Lee, K. S. Fancey, en J. Mi, "Non-destructive testing and evaluation of composite materials/structures: A state-of-the-art review", *Adv. Mech. Eng.*, vol 12, no 4, bll 1–28, 2020.

[2] M. Naebe, M. M. Abolhasani, H. Khayyam, A. Amini, en B. Fox, "Crack damage in polymers and composites: A review", *Polym. Rev.*, vol 56, no 1, bll 31–69, 2016.

[3] G. Neşer, "Polymer based composites in marine use: History and future trends", *Procedia Eng.*, vol 194, bll 19–24, 2017.

[4] S. Becz, J. Hurtado, en I. Lapczyk, "Analysis of barely visible impact damage for aerospace structures", *ICCM Int. Conf. Compos. Mater.*, no 1, bll 1–8, 2007.

[5] S. Mukherjee, X. Shi, L. Udpa, S. Udpa, Y. Deng, en P. Chahal, "Design of a Split-Ring Resonator Sensor for Near-Field Microwave Imaging", *IEEE Sens. J.*, vol 18, no 17, bll 7066–7076, 2018.

[6] O. Idolor, R. D. Guha, K. Berkowitz, C. Geiger, M. Davenport, en L. Grace, "Polymer-water interactions and damage detection in polymer matrix composites", *Compos. Part B Eng.*, vol 211, 2021.

[7] H. TOWSYFYAN, A. BIGURI, R. BOARDMAN, en T. BLUMENSATH, "Successes and challenges in non-destructive testing of aircraft composite structures", *Chinese J. Aeronaut.*, vol 33, no 3, bll 771–791, 2020.

[8] A. Kapadia, "Non-Destructive Testing of Composite Materials", *Handb. Multiph. Polym. Syst.*, vol 1, bll 777–796, 2011.

[9] A. Haque en M. K. Hossain, "Effects of moisture and temperature on high strain rate behavior of S2-glass-vinyl ester woven composites", *J. Compos. Mater.*, vol 37, no 7, bll 627–647, 2003.

[10] A. Katunin, A. Wronkowicz-Katunin, en D. Wachla, "Impact damage assessment in polymer matrix composites using self-heating based vibrothermography", *Compos. Struct.*, vol 214, no February, bll 214–226, 2019.

[11] P. Duchene, S. Chaki, A. Ayadi, en P. Krawczak, "A review of non-destructive techniques used for mechanical damage assessment in polymer composites", *J. Mater. Sci.*, vol 53, no 11, bll 7915–7938, 2018.

[12] M. Jolly *et al.*, "Review of Non-destructive Testing (NDT) Techniques and their Applicability to Thick Walled Composites", *Procedia CIRP*, vol 38, bll 129–136, 2015.

[13] C. Garnier, M. L. Pastor, F. Eyma, en B. Lorrain, "The detection of aeronautical defects in situ on composite structures using non destructive testing", *Composite Structures*, vol 93, no 5. bll 1328–1336, 2011.

[14] S. Gholizadeh, "A review of non-destructive testing methods of composite materials", in *Procedia Structural Integrity*, 2016, vol 1, bll 50–57.

[15] R. H. Bossi en V. Giurgiutiu, *Nondestructive testing of damage in aerospace composites*. Elsevier Ltd, 2015.

[16] S. Mukherjee, A. Tamburrino, L. Udpa, en S. Udpa, "NDE of composite structures using microwave time reversal imaging", *AIP Conf. Proc.*, vol 1706, no February 2016, 2016.

[17] L. A. Rodriguez, C. García, en L. R. Grace, "Long-term durability of a water-contaminated quartz-reinforced bismaleimide laminate", *Polym. Compos.*, vol 39, no 8, bll 2643–2649, 2018.

[18] O. Idolor, R. Guha, en L. Grace, "A dielectric resonant cavity method for monitoring of damage progression in moisture-contaminated composites", *33rd Tech. Conf. Am. Soc. Compos. 2018*, vol 2, bll 756–768, 2018.

[19] O. Idolor, R. Guha, L. Bilich, en L. Grace, "2-dimensional mapping of damage in moisture contaminated polymer composites using dielectric properties", in *Proceedings of the American Society for Composites - 34th Technical Conference, ASC 2019*, 2019.

[20] O. Idolor, R. Guha, K. Berkowitz, en L. Grace, "Damage Detection in Polymer Matrix Composites By Analysis of Polymer-Water Interactions Using Near-Infrared Spectroscopy", in *Proceedings of the American Society For Composites: Thirty-Fifth Technical Conference*, 2021.

[21] R. D. Guha, O. Idolor, en L. Grace, "Molecular Dynamics (MD) Simulation of a Polymer Composite Matrix with Varying Degree of Moisture: Investigation of Secondary Bonding Interactions", in *Proceedings of the American Society for Composites: Thirty-Fourth Technical*

Conference, 2019.
[22] O. Idolor, R. D. Guha, K. Berkowitz, en L. Grace, "An experimental study of the dynamic molecular state of transient moisture in damaged polymer composites", *Polym. Compos.*, 2021.
[23] R. D. Guha, O. Idolor, K. Berkowitz, M. Pasquinelli, en L. R. Grace, "Exploring secondary interactions and the role of temperature in moisture-contaminated polymer networks through molecular simulations", *Soft Matter*, vol 17, no 10, bll 2942–2956, 2021.
[24] R. D. Guha, O. Idolor, en L. Grace, "An atomistic simulation study investigating the effect of varying network structure and polarity in a moisture contaminated epoxy network", *Comput. Mater. Sci.*, vol 179, no January, bl 109683, 2020.
[25] L. R. Grace, "The effect of moisture contamination on the relative permittivity of polymeric composite radar-protecting structures at X-band", *Compos. Struct.*, vol 128, bll 305–312, 2015.
[26] G. Technique, C. Materials, en S. Gravity, "Standard Test Methods for Constituent Content of Composite Materials 1", bll 1–11, 2013.
[27] ASTM standard, "ASTM D 5229– 92 – Standard Test Method for Moisture Absorption Properties and Equilibrium Conditioning of Polymer Matrix Composite Materials", *Annu. B. ASTM Stand.*, vol 92, no Reapproved, bll 1–13, 2010.
[28] J. Krupka, A. P. Gregory, O. C. Rochard, R. N. Clarke, B. Riddle, en J. Baker-Jarvis, "Uncertainty of complex permittivity measurements by split post dielectric resonator technique.pdf". Journal of the European Ceramic Society 21, bll 2673–2676, 2001.
[29] T. P. Bagchi, *Multiobjective Scheduling by Genetic Algorithms*, no September. 1999.